PHYSICAL REVIEW B VOLUME 39, NUMBER 10 1 APRIL 1989

Density-functional theory of crystal-melt interfaces

W. A. Curtin
BP Research, 4440 Warrensville Center Road, Cleveland, Ohio 44128
(Received 28 November 1988)

The equilibrium structure and energetics of the crystal-melt interfaces of simple systems are studied using the nonlocal weighted density-functional approximation (WDA) to the Helmholtz free energy. The WDA, previously used to accurately predict bulk phase coexistence at the melting point, is combined with a new flexible, two-parameter parametrization of the crystal-melt interfacial region to predict interfacial properties. The parametrization allows for variations in the width of the interface and in the rate of broadening of the sharp density peaks of the crystal through the interface at fixed width, generating physically appealing profiles similar to those observed in simulation studies. The WDA in tandem with this parametrization thus avoids the use of the perturbation and/or square-gradient expansions previously used to describe both the crystal and the interface. Applying the approach to the model hard-sphere system (diameter σ), the (100) and (111) fcc-liquid interfaces are found to be four atomic layers in width and nearly isotropic in surface free energy γ, with $\gamma(100)=0.66kT/\sigma^2$ and $\gamma(111)=0.63kT/\sigma^2$. These results and the general interfacial structure are in qualitative agreement with simulation studies on the similar soft-sphere (r^{-12}) potential system. Using a simple hard-sphere perturbation theory, the crystal-liquid phase coexistence and (111) interface of the Lennard-Jones system are also examined. Both the freezing transition and the interfacial properties are dominated by the hard-core interactions, and the predicted value of $\gamma(111)=0.43\varepsilon/\sigma^2$ near the triple point is in reasonable agreement with the recent simulation result of $0.35\varepsilon/\sigma^2$. A brief comparison of the present "liquid" and the usual self-consistent phonon approaches to the crystal thermodynamics brings out some previously unrecognized similarities.

I. INTRODUCTION

The properties of the interface between a crystal and its melt are crucial to the understanding of many growth phenomena. For example, the interfacial free energy and its dependence on crystal orientation determine the equilibrium crystal shape[1] and the stability of a flat growing interface with respect to perturbations such as dendrite formation.[2] The interfacial free energy also governs the homogeneous nucleation of crystals in their melt and vice versa.[3] The atomic structure of the interface, either sharp or diffuse, can indicate the nature of some kinetic aspects of crystal growth.[4] Despite the importance of crystal-melt interfaces, experimental studies are difficult because the interface is confined between two dense phases and is not easily probed. The determination of the surface free energy γ is thus often made by rather indirect methods. Turnbull measured the maximum supercooling in small particles and then used the results of homogeneous nucleation theory to obtain values of γ for a wide variety of materials.[3] Aside from being an orientationally averaged value of γ, this approach depends crucially on purity and homogeneity in addition to the validity of the nucleation theory and its attendant limitations. More recent studies have relied on observing crystal-liquid-grain boundary intersection angles. The seminal work by Glicksman and Vold using this technique indicated that bismuth has a nearly isotropic γ, but the accuracy is in general limited to a few percent.[5] Crystal faceting during growth is not sufficient to guarantee anisotropy in γ because of the possibility of anisotropic growth kinetics, which has recently been observed in molecular dynamics studies of the nominally isotropic Lennard-Jones system.[6] Present theories of dendritic growth require that *some* anisotropy in γ be present; however, even anisotropy of less than 5% (smaller than can be deduced experimentally) between close-packed faces is sufficient because of a strong dependence of the theory on γ (Ref. 7). The atomistic structure of any crystal-melt interfaces has not, to our knowledge, been tackled experimentally.

As a result of the limited experimental data available, computer simulation studies have been an important part of the effort to understand crystal-melt interfaces. Early work involved using a static ($T=0$) crystalline solid as a wall against which a liquid phase was placed.[8] The expected induced structure of the liquid was observed but actual crystal-melt interface properties could not, of course, be obtained. Subsequent simulations of the interfaces between dynamic, coexisting crystal and liquid phases have been made but obtaining "true" equilibrium is subtle, and rather large 3D systems are required to obtain sufficiently large surface areas. In addition, the interface can wander from its initial position as the simulation progresses and this should tend to broaden out the observed interface structure, although not have too much of an effect on calculated thermodynamic quantities such as γ. Monitoring these potential difficulties carefully, the simulation studies of (i) the Lennard-Jones fcc (111), (100), and (110) interfaces by Broughton and Gilmer,[9] (ii) the r^{-12} fcc (100) interface by Cape and Woodcock,[10] and (iii) the r^{-12} fcc (111) interface by Tallon,[11] have yielded

interesting results. Namely, the interfacial regions are not atomically sharp but nonetheless are only about 6 or 7 layers in width, with the interfacial structure and in-plane correlations intermediate between those of the coexisting phases. Some features such as an expansion of the (100) lattice plane distance through the interface are particularly notable. The surface free energy, which is much more difficult to obtain accurately than are structural details, is nearly isotropic for the LJ system, with $\gamma(111)=\gamma(110)=0.35\varepsilon/\sigma^2$ and $\gamma(100)=0.34\varepsilon/\sigma^2$ all within $\pm 0.02\varepsilon/\sigma^2$ (Ref. 9). For the r^{-12} (100) interface, a surface stress of $\gamma(100)=0.46\pm 0.1(kT/\varepsilon)^{1/6}kT/\sigma^2$ was obtained.[10] These values are rather different than earlier simulation estimates, which is indicative of the general difficulty of obtaining surface energies from what are really bulk 3D simulations. A quantitative comparison of our theory with these results is one of the primary goals of this work.

A variety of theoretical approaches to this problem have been made over the years, and the monograph by Woodruff provides a comprehensive review.[12] Until recently, theories focused on either the structure of the interface or on its surface (free) energy but rarely on both simultaneously. The main debate in the 1950's and 1960's regarded the structure of the interface and the resultant growth morphology. For atomically smooth, or sharp, interfaces growth is thought to be limited to an activated layer-by-layer mechanism whereas for rough, or diffuse, interfaces growth can proceed in a continuous manner since many types of "surface" sites are available for liquid atoms impinging onto the solid surface. To predict which of these occurs for a particular material, the theory of Jackson assumed a lattice model with atoms on each site designated as either solid or liquid.[4] The interplay between the energy associated with the higher binding energy of a (nearly) full layer of solid particles and the entropy associated with the disorder of a partially solid, partially liquid layer at the interface determines the preferred morphology. Jackson found that rough interfaces are predicted if the key parameter $\alpha=\Delta H\nu/kT_{\rm melt}$, where ΔH is the latent heat of transition per particle and ν a face-dependent geometric factor less than unity, is smaller than about 2. This result is in rather remarkable agreement with experimental growth studies, which show faceted growth for high-α materials and continuous growth for low-α materials. The success of this simple theory led to extensions of it to broader interfaces and binary alloys. However, the surface free energies were not investigated in these studies and, in fact, attempts to account for the entropy via the Jackson-type models apparently lead to negative surface tensions.[12] Also, the lattice model could not adequately account for the true liquid structure.

Generally, early attempts to calculate interfacial energies were based on "broken-bond" models and used either the latent heat or internal energy as a measure of bond strength, as in Jackson's model. Entropy contributions, which we will see shortly to be actually quite large, were usually neglected. The work of Ewing is a notable exception.[13] Ewing recognized that a liquid in contact with a static solid or wall would become highly structured and that this structure would lower the entropy of the liquid. To estimate the excess configurational entropy of the nonuniform system, which can be expressed in terms of the density profile $\rho(\mathbf{r})$ as $S_{\rm conf}=-\int d\mathbf{r}\,\rho(\mathbf{r})\ln[\rho(\mathbf{r})/\rho_l]$, with ρ_l the asymptotic liquid density, he assumed the density perpendicular to the wall to be $\rho(z)=\rho_l g(r=z)$. Here, $g(r)$ is the radial distribution function of the *bulk* liquid and is identical to the structure induced in the liquid by the introduction of a fixed test particle at $r=0$. Applying this procedure to Au, Ewing found the entropic contribution to γ to be about $\frac{1}{2}$ of the total γ, the remainder accounted for by an additional $\Delta H/4$ per atom representing the "broken-bond" internal energy. Another approach to estimating γ was based on the "liquidlike" nature of large-angle grain boundaries; these boundaries were assumed to be back-to-back crystal-liquid interfaces and hence $\gamma_{XL}=\gamma_{GB}/2$ (Ref. 12). Generally, however, since these two interfaces are so close together, interaction effects between them imply that this estimate is an upper limit to γ_{XL}.

The major barrier to further theoretical progress at this time was the inability to describe both coexisting equilibrium phases, crystal and melt, accurately and within a compatible framework. Lattice models of the liquid were clearly deficient. And, while dislocation theories,[14] Lindemann criteria,[15] and self-consistent phonon calculations of crystal instabilities[16] could provide estimates of the melting point, a determination of true phase coexistence with a realistic liquid phase was not possible. The recent and rapid development of the theory of simple liquids finally allowed for fairly accurate calculations of equilibrium melting curves, as typified by the work of Stroud and Ashcroft.[17] However, the use of self-consistent phonon theory for the crystal, in which the crystal periodicity is crucial, and of liquid-state theory, in which the liquid translational invariance is key, are incompatible; the crystal-melt interface possesses neither the crystal nor liquid symmetry and a theory for it cannot be formulated by combining these two approaches (which are, nonetheless, highly successful for their appropriate phases).

The above impasse was largely broken by the pioneering work of Ramakrishnan and Youssouff (RY), who formulated a theory for the crystal thermodynamics based on liquid-state ideas and input.[18] In this theory, which was nicely reformulated into the language of (inhomogeneous) liquid theory by Haymet and Oxtoby (HO) (Ref. 19), the crystal is viewed as a highly inhomogeneous liquid with a spatially varying density $\rho_s(\mathbf{r})$ having the symmetry of the crystalline lattice. The viability of this view of the crystalline state is based on the density functional theorems of classical systems,[20] which state that thermodynamic quantities such as the Helmholtz free energy F are unique functionals of the density $\rho(\mathbf{r})$, $F=F[\rho(\mathbf{r})]$. Moreover, the equilibrium structure of the system is that which minimizes the grand potential functional $\Omega[\rho(\mathbf{r})]=-PV=F[\rho]-\mu N$. To make this a practical approach to obtaining the crystal thermodynamics, RY and HO assumed that a truncated expansion of the crystalline excess Helmholtz free energy, $F_{\rm ex}[\rho_s(\mathbf{r})]$,

about that of the liquid, $F_{ex}(\rho_l)$, in powers of $\rho_s(\mathbf{r})-\rho_l \equiv \Delta\rho(\mathbf{r})$ was valid,

$$F_{ex}[\rho_s(\mathbf{r})]=F_{ex}(\rho_l)-c^{(1)}(\rho_l)\int d\mathbf{r}\,\Delta\rho(\mathbf{r}) -\tfrac{1}{2}\int d\mathbf{r}\,d\mathbf{r}'c^{(2)}(\mathbf{r}'-\mathbf{r};\rho_l)\Delta\rho(\mathbf{r})\Delta\rho(\mathbf{r}') . \quad (1)$$

Here, $-c^{(1)}(\rho_l)$ is the excess chemical potential of the liquid and $c^{(2)}$ is the Ornstein-Zernike direct correlation function of the liquid. Input to the theory is thus liquid-state information *only* and the functional expansion becomes exact in the $\Delta\rho(\mathbf{r}) \ll 1$ limit. As such, the theory is essentially a sophisticated extension of Landau's theory of first-order phase transitions with an "order parameter" $\rho(\mathbf{r})$ taking on the value ρ_l=constant in the liquid and the form of $\rho_s(\mathbf{r})$ in the crystal. The predictions of the theory, embodied by Eq. (1) and a few auxiliary assumptions, for coexistence densities, pressure, and latent heat are generally quite good for a variety of systems where the liquid-state data is available.[21] These successes have led to applications of basic and modified versions of the theory to, for example, glasses,[22] quasicrystals,[23] crystal elastic constants,[24] and dislocations.[25]

Most important for the present discussion of interfaces is the natural extension of the basic theory made by Haymet and Oxtoby to study the interfaces between the two predicted coexisting phases.[19] In the simplest terms, the interface problem is no more difficult than the crystal problem, only the density profile $\rho(\mathbf{r})$ is different: the interface profile takes on the solid profile $\rho_s(\mathbf{r})$ and the liquid profile ρ_l asymptotically on either side of the interface. The functional to be minimized is not Ω=PV but the *excess* grand potential

$$\Delta\Omega=F[\rho(\mathbf{r})]-\mu\int d\mathbf{r}\,\rho(\mathbf{r})+\mathrm{PV} \quad (2)$$

subject to the asymptotic density constraints. The interfacial free energy γ is precisely $\Delta\Omega/A$ and thus emerges simultaneously with the interfacial structure and also naturally depends on the crystalline orientation. Haymet and Oxtoby utilized the truncated expansion Eq. (1) for the general $F_{ex}[\rho(\mathbf{r})]$ and made an additional square-gradient approximation for the variation of $\rho(\mathbf{r})$ through the interface. For the (100) and (111) faces of a bcc crystal, they obtained very broad interfaces, 10–15 atomic layers in width, validating the use of the square-gradient approximation. Values for the surface free energy of Na were about $\frac{1}{2}$ of those measured by Turnbull,[3] with an anisotropy of less than 3%. Subsequent studies of both bcc and fcc interfaces using slightly modified versions of Eq. (1) and usually with the auxiliary square-gradient approximation have been made by various workers and we will discuss these approaches in Sec. V.

In spite of the general success obtained using density-functional theory, a major problem remains regarding the expansion of Eq. (1). Namely, Eq. (1) is a truncated functional expansion in powers of $\rho_s(\mathbf{r})-\rho_l$ and such a perturbation theory is naturally suspect in application to crystals, where $\rho_s(\mathbf{r})$ is extremely rapidly varying (the crystal particles are highly localized about the lattice sites) and $\rho_s(\mathbf{r})-\rho_l \ll 1$ does not hold. In fact, the only attempt to include the next higher-order term in the expansion of F_{ex} yields rather poor predictions for the hard-sphere crystal-liquid coexistence conditions.[26] Also, the predicted crystal density peaks are much sharper than found in simulation studies and the consequences of such an unrealistic solid structure have an unknown but potentially large influence on the predicted interfacial properties. These concerns have motivated several groups to propose alternative, nonperturbative approximations to the functional $F_{ex}[\rho(\mathbf{r})]$ which include the higher-order terms neglected in Eq. (1) in an approximate manner. We will focus here on the weighted-density approximation (WDA) proposed by Curtin and Ashcroft that has been used with success to study hard sphere[27] and Lennard-Jones freezing.[28] The WDA is not perturbative and yields broader crystal peak widths and better bulk coexistence conditions than does the RY-HO theory, suggesting an improved description of the interface over predictions utilizing Eq. (1). The theory of Baus and co-workers, while quite successfully predicting bulk-phase coexistence, requires crystal-structure dependent input for the crystal phase.[29] Thus, it cannot be immediately employed to study interfaces, an additional local or square-gradientlike approximation for some key quantities appears necessary in this approach. The WDA does not suffer from this shortcoming and has, in fact, been applied to a host of nonfreezing problems involving liquids in contact with static walls to predict wetting phenomena and layering.[30]

The other approximation made by HO, the square-gradient approximation (SGA), is not necessary. The SGA merely simplifies the Euler-Lagrange equation which must be solved to obtain the equilibrium interfacial properties. Furthermore, since the fcc interfaces observed via simulations[9–11] are not particularly broad the SGA is not *a priori* applicable to crystal-melt interfaces. An alternative to solving the E-L equation which explicitly avoids any assumptions of slow variations of the interface is that of direct numerical minimization of Eq. (2) with respect to some parameters in an appropriate class of variational density profiles for the interface. The practical obstacle to this approach is the actual construction of realistic density profiles with a modest number of parameters. A major contribution of the present work is the description of a two-parameter class of interfacial density profiles which embodies the key feature expected in the true physical interface, namely the smooth broadening of the sharp crystal density peaks into the uniform liquid as the interface is traversed. The two parameters control the interface width and rate of broadening of the density peaks, respectively, and reproduce an often-used parametrization when no broadening is allowed. The features of this parametrization and general arguments indicate that even if the full interface is "broad," some Fourier components of $\rho(\mathbf{r})$ must actually vary much more rapidly and cannot be treated by SGA.

As mentioned in the preceding remarks, in this paper we apply the weighted-density approximation and a new, flexible parametrization of the interfacial region to predict the interfacial structure and surface free energies of several simple liquid systems. The combination of these two aspects overcomes most of the major drawbacks of

previous density-functional approaches to the study of crystal-melt interfaces and yields both structure and energetics in quantitative agreement with the accurate simulation results presently available. We concentrate on the hard-sphere system which has not been studied via simulation but is closely related to the purely repulsive r^{-12} potential system. Both the (100) and (111) fcc-liquid interfaces are found to be four atomic layers wide and the surface free energy is nearly isotropic, with $\gamma(111)=0.63kT/\sigma^2$ and $\gamma(100)=0.66kT/\sigma^2$ ($\pm 0.02\ kT/\sigma^2$). In a simple but useful extension to the Lennard-Jones system, we find similar widths and $\gamma=0.43\varepsilon/\sigma^2$ near the triple point. A partial description of the present work which studied only the hard-sphere (100) interface has previously been published.[31]

The remainder of this paper is organized as follows. In Sec. II we review density-functional theory and introduce the WDA as an approximate free energy functional for inhomogeneous systems. In Sec. III the bulk crystal-liquid phase coexistence of the hard-sphere system is calculated using the WDA. Then, a simple extension to the Lennard-Jones crystal is presented and some similarities between the density-functional approach taken here and the self-consistent Debye approach to crystal thermodynamics are revealed. The main part of this paper is Sec. IV, in which our new density parametrization is presented and the results of interfacial calculations are given for the hard sphere and Lennard-Jones systems. Finally, in Sec. V we discuss previous DF treatments of the interface, the limitations of the present approach, and extensions of the theory to other interfaces. The Appendix contains a few details on the numerical procedures employed here.

II. DENSITY-FUNCTIONAL THEORY AND THE WEIGHTED DENSITY APPROXIMATION

Consider a system of monoatomic particles which interact through pairwise potential $\phi(r)$ and are in an external field $V_{\rm ext}(r)$. For N atoms in a volume V the microscopic Hamiltonian is thus

$$H=\sum_i P_i^2/2M+\tfrac{1}{2}\sum_{i\neq j}\phi(\mathbf{r}_i-\mathbf{r}_j)+\sum_i V_{\rm ext}(\mathbf{r}_i)\ . \tag{3}$$

At a temperature T ($\beta=1/kT$) and single particle density $\rho(\mathbf{r})$ (average of the density operator $\hat{\rho}$), the grand potential functional $\Omega[\rho]$ and Helmholtz free energy functional $F[\rho]$ are unique functionals of the density $\rho(\mathbf{r})$, as shown by Mermin.[20,32] Ω and F are related by

$$\Omega[\rho]=F[\rho]-\mu\int d\mathbf{r}\,\rho(\mathbf{r})+\int d\mathbf{r}\,\rho(\mathbf{r})V_{\rm ext}(\mathbf{r})\ , \tag{4}$$

where μ is the chemical potential. The equilibrium density $\rho_0(\mathbf{r})$ for the system is found by minimizing the grand potential functional with respect to variations in $\rho(\mathbf{r})$,

$$\left.\frac{\delta\Omega}{\delta\rho(\mathbf{r})}\right|_{\rho(\mathbf{r})=\rho_0}=0\ . \tag{5}$$

At the equilibrium density, $\Omega[\rho_0]$ and $F[\rho_0]$ are the grand potential ($-PV$) and Helmholtz free energy, respectively, of the system.

The Helmholtz free energy functional F consists of two contributions, (i) an ideal gas part $F_{\rm id}$ which accounts for the entropy cost of establishing a nonuniform density $\rho(\mathbf{r})$ even in the absence of interparticle interactions, and (ii) an excess contribution $F_{\rm ex}$ due to interactions. Writing F as

$$\begin{aligned}F[\rho]&=F_{\rm id}+F_{\rm ex}\\&=\beta^{-1}\int d\mathbf{r}\,\rho(\mathbf{r})\{\ln[\rho(\mathbf{r})\Lambda^3]-1\}+F_{\rm ex}[\rho]\end{aligned} \tag{6}$$

(with Λ the thermal wavelength), the equilibrium density $\rho_0(\mathbf{r})$ must then satisfy the self-consistent equation

$$\rho_0(\mathbf{r})=\Lambda^{-3}\exp[\beta\mu+c^{(1)}(\mathbf{r};\rho_0(\mathbf{r}))-\beta V_{\rm ext}(\mathbf{r})]\ . \tag{7}$$

Here,

$$\beta^{-1}c^{(1)}(\mathbf{r};\rho)=-\delta F_{\rm ex}[\rho]/\delta\rho(\mathbf{r}) \tag{8}$$

is precisely the one-body self-consistent potential created by the interacting particles in the configuration $\rho(\mathbf{r})$ and which therefore determines the equilibrium density profile. $c^{(1)}$ is the first in a hierarchy of direct correlation functions $c^{(n)}$, for which $F_{\rm ex}[\rho]$ is the generating functional:

$$c^{(n)}(\mathbf{r}_n\cdots\mathbf{r}_1)=-\beta\frac{\delta F_{\rm ex}^n[\rho]}{\delta\rho(\mathbf{r}_n)\cdots\delta\rho(\mathbf{r}_1)}\ . \tag{9}$$

The $c^{(n)}$ of the *homogeneous* liquid [$\rho(\mathbf{r})=\rho$] also satisfy the sum rule

$$\int d\mathbf{r}_n c^{(n)}(\mathbf{r}_n\cdots\mathbf{r}_1;\rho)=\frac{\partial c^{(n-1)}}{\partial\rho}(\mathbf{r}_{n-1}\cdots\mathbf{r}_1;\rho)\ . \tag{10}$$

Because of the relations given by Eqs. (8) and (9) and the uniqueness of $F[\rho]$, we may obtain $F_{\rm ex}[\rho]$ by functionally integrating Eqs. (8) and (9) along an arbitrary path from some reference density ρ_R (chose to be uniform) up to the desired density $\rho(\mathbf{r})$. Choosing a linear path, we obtain

$$\begin{aligned}F_{\rm ex}[\rho]=F_{\rm ex}(\rho_R)&-\beta^{-1}c^{(1)}(\rho_R)\int d\mathbf{r}[\rho(\mathbf{r})-\rho_R]\\&-\tfrac{1}{2}\beta^{-1}\int d\mathbf{r}'d\mathbf{r}[\rho(\mathbf{r}')-\rho_R][\rho(\mathbf{r})-\rho_R]\\&\times\int_0^1 d\alpha(1-\alpha)c^{(2)}(\mathbf{r},\mathbf{r}';\rho(\alpha))\ ,\end{aligned} \tag{11}$$

where $c^{(2)}(\mathbf{r},\mathbf{r}';\rho(\alpha))$ is the d.c.f of the inhomogeneous system of density $\rho(\alpha)=\rho_R+\alpha[\rho(\mathbf{r})-\rho_R]$.

Equation (11) is the starting point for a number of approximations for $F_{\rm ex}[\rho]$. For example, by selecting $\rho_R=\rho_l$ (the coexisting liquid density) and expanding $c^{(2)}(\mathbf{r},\mathbf{r}';\rho(\alpha))$ about $\alpha=0$ to $O(\alpha^0)$, the RY-HO functional Eq. (1) is obtained.[19,20] By Eqs. (8) and (9), this is also simply a functional expansion of $F_{\rm ex}[\rho]$ about $F_{\rm ex}(\rho_l)$ truncated at second order. On the other hand, selecting $\rho_R=0$ and rearranging gives the form

$$F_{\rm ex}[\rho]=\int d\mathbf{r}\,\rho(\mathbf{r})f[\mathbf{r};\rho(\mathbf{r})]\ , \tag{12}$$

where

$$\begin{aligned}f[\mathbf{r};\rho(\mathbf{r})]=-\tfrac{1}{2}\beta^{-1}&\int d\mathbf{r}'\rho(\mathbf{r}')\\&\times\int_0^1 d\alpha(1-\alpha)c^{(2)}(\mathbf{r},\mathbf{r}';\rho(\alpha))\end{aligned} \tag{13}$$

is the free energy contribution at $\mathbf{r}$ and is a *nonlocal functional* of the density $\rho(\mathbf{r})$. Since (13) involves $c^{(2)}$, which has a spatial extent comparable to that of $\phi(\mathbf{r})$, $f[\mathbf{r};\rho(\mathbf{r})]$ is nonlocal on the same length scale.

The weighted-density approximation[27] (WDA) replaces $f[\mathbf{r};\rho(\mathbf{r})]$ in (12) by a *function* of a *nonlocal* density, specifically

$$f[\mathbf{r};\rho(\mathbf{r})]\approx f(\bar{\rho}(\mathbf{r}))\ , \tag{14}$$

where $f(\rho)$ is the Helmholtz free energy per particle of a *uniform liquid* and $\bar{\rho}(\mathbf{r})$ is a nonlocal density. The nonlocal density $\bar{\rho}(\mathbf{r})$ is taken to be a self-consistent weighted average of the real density $\rho(\mathbf{r})$:

$$\bar{\rho}(\mathbf{r})=\int d\mathbf{r}'\rho(\mathbf{r}')w(\mathbf{r}'-\mathbf{r};\bar{\rho}(\mathbf{r}))\ . \tag{15}$$

The weighting function w in Eq. (15) is then determined by demanding that the resulting WDA functional

$$F_{\rm ex}^{\rm WDA}[\rho]=\int d\mathbf{r}\rho(\mathbf{r})f(\bar{\rho}(\mathbf{r}))\ , \tag{16}$$

(i) be exact in the uniform liquid limit $\rho(\mathbf{r})=\rho$, which simply requires w to be normalized, and (ii) satisfy Eq. (9) *exactly* in the uniform liquid limit [Eq. (8) already being satisfied in this limit if w is normalized]. Thus, equating the second functional derivative of $F_{\rm ex}^{\rm WDA}$ in the liquid limit to $c^{(2)}(\mathbf{r};\rho)$, the liquid direct correlation function, yields the following equation for $w(k;\rho)$ after Fourier transformation:

$$\beta^{-1}c^{(2)}=-2\frac{\partial f}{\partial\rho}-\rho\frac{\partial^2 f}{\partial\rho^2}w^2-2\rho\frac{\partial f}{\partial\rho}w\frac{\partial w}{\partial\rho}\ . \tag{17}$$

Solving for w shows it to have about the same spatial range as $c^{(2)}$, naturally, and hence $f(\bar{\rho}(\mathbf{r}))$ is nonlocal on the same scale as $f[\mathbf{r};\rho]$ (Ref. 27).

With the above prescription for $F_{\rm ex}^{\rm WDA}[\rho]$ several key aspects are worthy of discussion. First, $F_{\rm ex}^{\rm WDA}$ is nonperturbative and does not assume variations in $\rho(\mathbf{r})$ to be small. Second, if a functional expansion of $F_{\rm ex}^{\rm WDA}[\rho]$ about any uniform density ρ_0 is performed, the expansion is exact to second order *by construction* and higher-order terms involving *approximate* liquid higher-order d.c.f.'s $c_{\rm WDA}^{(n)}(\mathbf{r}_n\ldots\mathbf{r}_1;\rho)$ $n>2$ appear in the expansion. Moreover, because of the self-consistent determination of $\bar{\rho}(\mathbf{r})$ in Eq. (15), the approximate $c_{\rm WDA}^{(n)}$ satisfy the sum rule of Eq. (10) *exactly*. This latter point means that the WDA contains *all* information obtainable from the two-point function $c^{(2)}$ and retains an important relationship between $c^{(n)}$ and $c^{(n-1)}$. Any systematic improvements to the WDA will thus require knowledge of nontrivial three- and higher-particle correlation functions in the uniform liquid. In fact, the author and Ashcroft[33] have recently compared $c_{\rm WDA}^{(3)}$ to the detailed simulation data of Barrat *et al.*[34] and find fairly good agreement for the limited geometries studies. Based on this agreement, $c_{\rm WDA}^{(3)}$ has been used to extend the truncated functional expansion to third-order approximately, which yields rather poor hard-sphere coexistence conditions, thereby casting doubt on the validity of the second-order truncation.[26]

The WDA formulation makes no assumption that a crystalline phase is under investigation; the WDA is a general functional for inhomogeneous liquids. It has been applied in a variety of wetting studies, where the Tarazona formulation is used to obtain w approximately and the approach has been coined the smoothed-density approximation (SDA) (Ref. 30). The successful application of the WDA to the highly inhomogeneous crystalline phase, as discussed in the next section, suggests that it is capable of handling the interface problem where the density variations are necessarily less drastic. And, no additional approximations are required.

III. CRYSTAL-LIQUID COEXISTENCE: HARD-SPHERES AND LENNARD-JONES LIQUIDS

The crystalline state corresponds to a solution of the Euler-Lagrange equation, Eq. (7), with $V_{\rm ext}=0$ and $\rho(\mathbf{r})$ possessing the crystalline symmetry, which must be assumed *a priori*. Using the WDA functional, the one-body potential $c^{(1)}(\mathbf{r};\rho(\mathbf{r}))$ is, unfortunately, a rather unwieldy functional for the inhomogeneous system. Thus, we make use of the variational principle, formally exact for the true functional, and minimize the free energy with respect to variations in $\rho_s(\mathbf{r})$. Since the WDA is an approximation for F, it is most convenient to fix the average density $\rho_s=1/V\int d\mathbf{r}\rho_s(\mathbf{r})$ and minimize F with respect to spatial variations in $\rho_s(\mathbf{r})$. The chemical potential μ and pressure P are then obtained by the standard Legendre transformation

$$\mu=\frac{\partial}{\partial\rho_s}(F/V),\quad P=\rho_s\mu-F/V\ . \tag{18}$$

Finally, crystal-liquid coexistence is found by simultaneously equating μ, P, and T in the two phases.

For coexistence to occur, the Helmholtz free energies of the crystal and liquid must cross at some density. The stability of the crystal phase at higher densities (for materials which expand on melting) is accomplished by a trade-off between "ideal" and "excess" free energy contributions as follows. With increasing localization, the ideal contribution $F_{\rm id}$ is monotonically increasing. However, the excess contribution $F_{\rm ex}$ can be *decreasing* with increasing localization if the localized particles are less interacting, meaning that the coupling constant integral in Eq. (13) acts like a mean-field, structure-dependent pair potential which can favor highly localized particles. This competition between $F_{\rm id}$ and $F_{\rm ex}$ can yield a local minimum in F at finite localization, a phase we identify as the stable or metastable crystal phase. Once a local minimum appears, it becomes deeper (the crystal becomes more stable relative to the isochoric liquid) with increasing average density.

For the calculations to follow, the variational class of crystal densities is restricted to the now common form of isotropic Gaussian peaks centered on the lattice sites R,

$$\rho_s(\mathbf{r})=\left[\frac{\alpha}{\pi}\right]^{3/2}\sum_R e^{-\alpha(\mathbf{r}-R)^2}\ , \tag{19}$$

with the single variational parameter α determining the peak widths. Equation (19) includes a wide range of profiles, including the liquid state ($\alpha=0$) and the zero-temperature crystal ($\alpha=\infty$). α is inversely proportional

to the mean-square displacement of the solid particles and at phase coexistence is thus related to the Lindemann parameter L by $L=(3/\alpha\sigma^2)^{1/2}$ for the fcc lattice. The form of Eq. (19) is identical to that assumed in a self-consistent Debye model of the crystal (see Sec. III C), in which the Debye temperature Θ_D is the single variational parameter and is related to our α by $\Theta_D/T=(3\alpha/\pi)^{1/2}\Lambda$. A more general parametrization in which the magnitudes of the reciprocal lattice vector Fourier components ρ_G are variational parameters,

$$\rho_s(\mathbf{r})=\rho_s+\sum_{G\neq 0}\rho_G e^{i\mathbf{G}\cdot\mathbf{r}} \tag{20}$$

has been used in other DF theories with only minor deviations compared to Eq. (19) [which corresponds to $\rho_G=\rho_s\exp(-G^2/4\alpha)$]. In practice, the sum in Eq. (20) must be truncated at some level. Early workers using Eq. (1) included only the smallest one or two sets[18,19] of symmetry-related G vectors in bulk and interface calculations and subsequent work included an insufficient number of G vectors,[35] but the more recent efforts have insured that the level of truncation does not affect the bulk coexistence conditions.[36]

The procedure for finding F is now simply to fix ρ_s and search for local minima in $F_{\rm id}+F_{\rm ex}^{\rm WDA}$ with respect to α. For calculating the weighted densities $\bar{\rho}(\mathbf{r})$ via Eq. (15), the form of Eq. (20) is most convenient since w is most easily obtained in Fourier space. Thus, we have

$$\bar{\rho}(\mathbf{r})=\rho_s+\sum_{G\neq 0}\rho_G w(G;\bar{\rho}(\mathbf{r}))e^{i\mathbf{G}\cdot\mathbf{r}}\ , \tag{21}$$

and for all the results reported below the sum includes all G vectors satisfying $|\mathbf{G}|\leq(72)^{1/2}2\pi/a$, where a is the cubic lattice spacing. Self-consistency is rapidly obtained by a simple iterative process. As an aside, using Eq. (19) the ideal gas contribution $F_{\rm id}$ is accurately approximated for large α ($\alpha\sigma^2\gtrsim 50$) by the simple expression

$$\beta F_{\rm id}/N=\tfrac{3}{2}\ln\left[\frac{\alpha}{\pi}\right]-\ln(\rho_s\Lambda^3)-\tfrac{5}{2}\ , \tag{22}$$

which shows the monotonic increase in "ideal" free energy due to increasing localization mentioned earlier.

A. The hard-sphere system

We now present results for the fcc hard-sphere crystal thermodynamics because the original calculations in Ref. 27 contain some minor numerical errors which have been corrected. As in Ref. 27 we use the Percus-Yevick approximation for $c^{(2)}$ of the liquid and the liquid equation of state and excess free energy f which are generated by the compressibility route to the liquid thermodynamics.[37] Thus, both $c^{(2)}$ and f are available in simple analytic form.

TABLE I. Hard-sphere fcc crystal free energy per particle $\beta F/N$ and pressure βP vs average density ρ_s.

	$\beta F/N$		βP	
$\rho\sigma^3$	WDA	Sim.	WDA	Sim.
1.00	4.449	4.661	8.83	10.26
1.025	4.674	4.868	9.64	11.11
1.05	4.908	5.099	10.60	12.12
1.075	5.155	5.354	11.89	13.20
1.10	5.422	5.663		

TABLE II. Hard-sphere fcc-liquid coexistence data.

	ρ_s	ρ_l	$\Delta s/k_b$	L	$\beta P/\rho_s$
WDA	1.02	0.881	1.46	0.101	9.28
Sim.	1.04	0.94	1.16	0.126	10.9

The fcc crystal Helmholtz free energy per particle, $\beta F/N$ and pressure βP are given in Table I over a wide range of densities. As shown previously, agreement with Monte Carlo simulation data is quite good, with deviations in the primary calculated quantity $\beta F/N$ being less than 5%. The derivative quantity βP shows slightly larger deviations. Nonetheless, the crystal-liquid coexistence properties, presented in Table II, are generally quite good. In particular, the closeness of the Lindemann parameter to its simulated value indicates that the predicted variations in $F_{\rm ex}^{\rm WDA}$ with α are roughly correct. So, the good agreement is not a fortuitous consequence of canceling errors being minimized by the variational procedure.

B. The Lennard-Jones system

In this section we consider the Lennard-Jones system by developing a very simple hard-sphere perturbation theory. The present approach is a simplification of a more refined theory[28] previously used to accurately calculate the full LJ phase diagram but makes the computational problem trivial if the hard-sphere crystal data is in hand.

For the general inhomogeneous liquid, we expand the free energy of the LJ potential system about that of reference hard-sphere (hs) system of diameter d as

$$F[\rho]=F_{\rm id}[\rho]+F_{\rm ex}^{\rm hs}[\rho]+\tfrac{1}{2}\int d\mathbf{r}\,d\mathbf{r}'\phi(\mathbf{r}'-\mathbf{r})\rho(\mathbf{r})\rho(\mathbf{r}')g_{\rm hs}(\mathbf{r}',\mathbf{r};\rho,d)\ , \tag{23a}$$

where $g_{\rm hs}(\mathbf{r}',\mathbf{r};\rho,d)$ is the pair-correlation function of the *inhomogeneous* hs reference system. By a simple change of variables in the last term of (23a) we may rewrite this as

$$F[\rho]=F_{\rm id}[\rho]+F_{\rm ex}[\rho]+\frac{N}{2}\int d\mathbf{r}\,\phi(\mathbf{r})\hat{g}_{\rm hs}(r;\rho,d)\ , \tag{23b}$$

where we have defined

$$\hat{g}_{\rm hs}(r;\rho,d)=\frac{1}{4\pi V}\int d\Omega\,d\mathbf{r}'\frac{\rho(\mathbf{r})\rho(\mathbf{r}')}{\rho\rho}g_{\rm hs}(\mathbf{r}+\mathbf{r}',\mathbf{r};\rho,d)\ , \tag{23c}$$

which is clearly a spherical average of the integrated

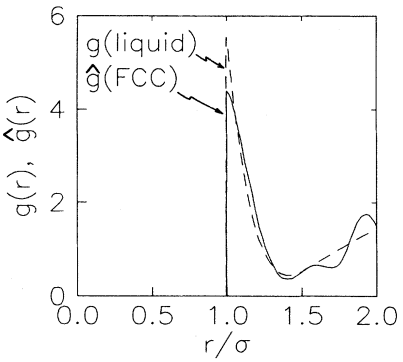

FIG. 1. Comparison of the liquid pair-correlation function g and the spherically averaged, integrated two-particle distribution function $\hat{g}$ [see Eq. (23c)] of the fcc crystal for the hard-sphere system of density $\rho\sigma^3=1.0$.

two-particle distribution function. Now for studying the crystal-liquid transition, two points are important to recognize. First, since freezing is dominated by the packing constraints governed by the short range, strongly repulsive interactions, the hs reference free energy contains most of the important physics. Second, the internal energy difference between equal density crystal and liquid phases is quite small, since both dense phases have neighboring particles near the minimum of the LJ potential well. These points motivate the simple approximation of replacing $\hat{g}_{\rm hs}(\mathbf{r};\rho,d)$ in Eq. (23b) by the *liquid* $g_{\rm hs}(r;\rho,d)$ at the same average density ρ (Ref. 38). The similarity between the liquid $g_{\rm hs}$ and the crystal $\hat{g}_{\rm hs}$ is shown in Fig. 1 for hard spheres at the density $\rho\sigma^3=1.0$, and the major difference is in the oscillations of $\hat{g}_{\rm hs}$ at long distances (where ϕ is small) (Ref. 39). With this Ansatz, the approximate free energy then becomes

$$F[\rho]=F_{\rm id}[\rho]+F_{\rm ex}^{\rm hs}[\rho]+\frac{N}{2}\rho\int d\mathbf{r}\,\phi(r)g_{\rm hs}(r;\rho,d)\ . \tag{24}$$

In the liquid limit, Eq. (24) is the standard hs perturbation expression. For the crystal, we have simply left out any structure-dependent internal energy contributions, which are expected to be small. Our previous work includes structural corrections to the crystal internal energy.[28]

To calculate the LJ fcc crystal free energy using Eq. (24), we make several auxiliary approximations. As in the hard-sphere case, we parametrize the density by Eq. (19). Then, since only $F_{\rm hs}[\rho]$ depends on $\rho_s(\mathbf{r})$, the minimization with respect to α has already been performed and the hs crystal free energies given in Table I are appropriate to the LJ crystal of density $\rho\sigma^3/d^3$. Next, we use the Percus-Yevick solution for $g_{\rm hs}$ and approximate $\phi_{\rm LJ}(r)$ by an extremely accurate fit using the Double Yukawa potential $\phi_{\rm DY}$, the combination of which allows the internal energy term in Eq. (24) to be calculated analytically.[40] Finally, we choose the diameter d in the simple manner suggested by Ashcroft and Langreth,[41]

$$\phi_{\rm DY}(d)=\tfrac{3}{2}kT-\varepsilon\ , \tag{25}$$

where ε is the potential well depth.

Crystal-liquid coexistence calculated using Eqs. (24) and (25) at several temperatures is presented in Table III along with the simulation results.[42,43] The triple point lies in the range $0.55<kT_t/\varepsilon<0.60$, a bit lower than simulation values. For reference, the liquid-vapor critical point, which only depends on the liquid limit of Eq. (24), is found to be at $kT_c/\varepsilon=1.35$ and $\rho_c\sigma^3=0.29$, compared to the values $kT_c/\varepsilon=1.35$ and $\rho_c\sigma^3=0.36$ found in simulation studies. Given the simplicity of this approach, the agreement is rather good, which indicates that the main approximation of neglecting the structure-dependent internal energy contributions is not unreasonable. Naturally, the agreement here is not as good as obtained earlier with the more sophisticated approach, but the present simplifications will allow for a rather easy assessment of the importance of attractive interactions in determining the interfacial free energy.

C. A comparison of liquid and phonon theories of the crystal

Now that we have extended the liquid-based theory of crystalline thermodynamics to non-hs systems, we may compare it to the self-consistent phonon theory of the crystal.[44] Although the phonon theory is not generally applicable to inhomogeneous liquids, it is a good approach to the crystal and it is of considerable interest to relate the apparently very different liquid-based approach to it. Our comparison is limited to comparing the density functional view of the crystal within a one-parameter (α) theory to a self-consistent Debye model, which is the one-parameter (Θ_D) theory for dynamic crystals starting from the usual phonon viewpoint.[45] The Debye model is obtained from the more general self-consistent phonon theory by assuming that the phonon frequency spectrum is $\omega=cq$, $q<q_D$, where q_D is related to the Debye temperature by $k\Theta_D=hcq_D$ and c is the sound velocity. The liquid-based theory is inherently a high-temperature theory and so we consider this regime only, which is

TABLE III. Lennard-Jones fcc-liquid coexistence data at various temperatures (simulation results in parentheses).

kT/ε	d/σ	ρ_s	ρ_l	L	P
0.67	1.000	1.015	0.882	0.102	1.27
0.75	0.995	1.025(0.973)	0.898(0.875)	0.103(0.145)	2.41(0.67)
1.15	0.976	1.059(1.024)	0.946(0.936)	0.112(0.139)	7.62(5.68)
1.35	0.969	1.085(1.053)	0.970(0.964)	0.122(0.137)	10.8(9.00)

characterized by $\Theta_D/T \ll 1$, so that quantum effects are negligible. Then, in both one-parameter theories, the crystal density is assumed to be Gaussian around each lattice site and α and Θ_D are related by $\Theta_D/T = (3\alpha/\pi)^{1/2}\Lambda$.

Now the crystal free energy consists quite generally of kinetic energy E, entropy S (both ideal and excess), and internal energy U. We consider these contributions in two parts. First, the kinetic energy and phonon entropy per particle in the polarization-independent Debye model are given by, in the notation of Ref. 17,

$$E = 9k\Theta_D/16 + 3kTI(\Theta_D/T)$$

and

$$-TS = kT[3\ln(1-e^{-\Theta_D/T}) - 4I(\Theta_D/T)] ,$$

where $I(x)$ is the Debye integral

$$I(x) = (3/x^3)\int_0^x t^3(e^t-1)^{-1}dt .$$

At high temperatures, we may expand the Debye integral in powers of Θ_D/T. Making use of the relation between Θ_D and α, the sum of the kinetic energy and phonon entropy terms for a crystal of density ρ is

$$\beta(E-TS) = \tfrac{3}{2}\ln(\alpha/\pi) + \ln(\rho\Lambda^3) - \tfrac{5}{2} + \tfrac{3}{2}\ln(3) ,$$

plus small corrections of order $(\Theta_D/T)^4$. This expression is nearly identical to the large α limit of the ideal gas free energy $\beta F_{\rm id}/N$ [see Eq. (22)], differing only by a constant $(\frac{3}{2})\ln(3)$. The constant does not affect the subsequent minimization of the free energy nor the value of the pressure. This close relationship is reasonable: At high temperature, the phonons in the Debye model are a collection of independent, classical oscillators while the ideal gas entropy of the inhomogeneous liquid is due to noninteracting (i.e., independent) particles in the presence of a harmonic one-body potential. The Debye model contains no *excess* entropy, however, and anharmonic effects are only included to the extent that the self-consistency aspect yields an effective harmonic system. In a system such as hard spheres, for which the free energy is entirely entropic, the anharmonic contributions are absolutely necessary to obtain a stable crystal phase. The liquid-based theory we have presented includes the anharmonic effects nonpertubatively via the use of the WDA, and near melting is expected to be superior to the more general self-consistent phonon theory, which includes anharmonic effects perturbatively. At lower temperatures, the excess entropy is less important and the self-consistent phonon theory should be better than the liquid-based theory.

The other contribution to the free energy in both theories is the internal energy, which may be expressed quite generally by

$$U/N = (\rho/2)\int d\mathbf{r}\,\phi(r)\hat{g}(r;\rho) .$$

The difference between the theories arises in the specification of $\hat{g}$. In the Debye model, the pair-correlation function is[17]

$$\hat{g}(r;\rho) = (1/\rho)\int d\Omega \sum_{\mathbf{R}\neq 0} \Gamma^{3/2}\exp[-\Gamma(\mathbf{r}-\mathbf{R})^2/2] .$$

Here, $\Gamma = \alpha(1-\Lambda_1)^{-1}$ and Λ_1 is given in the one phonon approximation by[17]

$$\Lambda_a(R) = (1/q_D R)\int_0^{q_D R} \sin(y)/y\,dy ,$$

which describes the correlations between a particle at the origin and a particle at the site R and it approaches zero at large R. In the liquid-based approach, we have motivated an approximation for the internal energy based on the similarity of the liquid g to the crystal $\hat{g}$: we assume the correlations to be mainly liquidlike. The Debye phonon model certainly provides a better estimate of the crystal correlation function, but at temperatures near melting the crystal and liquid internal energies are not all that different and the liquid approximation is adequate. Of course, the liquid-based approach could use the Debye form for $\hat{g}$ to study the crystal, but this loses its appeal when considering any noncrystalline inhomogeneous liquids (such as the crystal-liquid interface), and it is preferable to introduce structure-dependent corrections to U/N in the manner of Ref. 28.

Clearly, there are more similarities between the liquid-based and phonon theories of the crystal than first meets the eye. The ideal gas entropy and internal energy are basically common to both theories, although calculated within slightly different approximations. In the inclusion of excess entropy, or anharmonic effects, the theories differ considerably, so that the phonon theory is most appropriate at moderate temperatures while the liquid-based theory is probably more appropriate at melting.

IV. CRYSTAL-MELT INTERFACES

With the bulk-phase coexistence data as obtained in the previous section, we may now proceed to analyze the interfacial structure and energetics. The application of density-functional theory is straightforward, with interfacial thermodynamic quantities now of interest. The interfacial region takes on the density profile $\rho(\mathbf{r})$ which minimizes the excess Grand potential $\Delta\Omega$,

$$\Delta\Omega = F[\rho(\mathbf{r})] - \mu\int d\mathbf{r}\,\rho(\mathbf{r}) + PV \tag{26}$$

subject to the constraints $\rho(\mathbf{r}) = \rho_l$ and $\rho(\mathbf{r}) = \rho_s(\mathbf{r})$ asymptotically on either side of the interface and at the coexisting (μ, P, T). As noted in the Introduction, the surface free energy is then $\Delta\Omega/A$, A being the surface area, evaluated at the minimizing density $\rho(\mathbf{r})$.

A caveat to the application of density-functional theory to not only this but all liquid problems is that DFT is a mean-field theory. The density $\rho(\mathbf{r})$ is an average of the density operator $\hat{\rho}$ and no fluctuation corrections are included into the theory. For the strongly first-order freezing transition such fluctuations are likely negligible. But in studying interfacial problems, fluctuations can be important due to the existence of long-wavelength capillary waves, roughening transitions, etc. Such effects are completely neglected here, where we consider infinite planar interfaces only, and so we proceed in the manner of many earlier workers who have used DFT to study liquid-vapor interfaces.[46]

In analogy with the bulk-phase problem, the minimum of Eq. (26) may be found by solving the Euler-Lagrange

equation. For some of the less sophisticated approximations to F_{ex} used, an additional square-ingredient approximation allows for an analytic solution in which the density profile takes on the standard tanh form. For the WDA functional, and other approaches, the E-L equation does not simplify and the variational principle must again be utilized by parametrizing $\rho(\mathbf{r})$ and minimizing Eq. (26). Direct minimization has the advantage that the SGA is not invoked but the disadvantage that realistic and flexible parametrizations have not been available until now. So, in the remainder of this section we will first motivate and describe in some detail our parametrization of the interfacial density. We will then use it in a direct minimization of Eq. (26) with the WDA to analyze the (100) and (111) hard-sphere interfaces. Finally, we will consider the Lennard-Jones interface in the same framework.

A. Parametrization of the Crystal-Melt Interfacial Profile

In the crystal, each sharp density peak is maintained by the self-consistent potential generated by neighboring particles. If the averaged density or averaged order across a plane of particles is reduced, the self-consistent potential is naturally broadened relative to the full, perfect lattice. Conversely, structure is induced in an otherwise uniform dense liquid in the proximity of any type of external field (or wall) or, equivalently, the wall potential and interparticle potentials yield a self-consistent potential with minima near the wall. In the crystal-liquid interfacial region, the ultimate presence of the liquid on one side of the interface must serve to disorder or broaden the crystalline layers while the ultimate presence of the crystal lattice planes on the other side of the interface must induce some structure in the dense liquid. Thus, as the interface is traversed from crystal to liquid the very sharp density peaks characteristic of the crystal are expected to broaden in a smooth manner and ultimately strongly overlap and resemble the perturbed liquid. Of course, the number of atomic layers over which such a transition is expected to occur is unknown and could be quite few for a "sharp" interface. How the peaks broaden through the interface is also unknown. A useful parametrization of the interface should incorporate these general physical features as well as allow for possible lattice plane expansion or contraction and anisotropic features.

A simple, appealing possibility is to generalize the parameter α in Eq. (19), allowing it to vary as a function of distance z perpendicular to the interface, $\alpha=\alpha(z)$. At the same time, however, the average density must change from ρ_s to ρ_l while maintaining $\rho(\mathbf{r})\geq 0$ everywhere. The latter constraint makes such an approach somewhat complicated. A choice which does guarantee $\rho(\mathbf{r})\geq 0$ is $\rho(\mathbf{r})=\rho_l+f(z)\,[\rho_s(\mathbf{r})-\rho_l]$ with $0\leq f(z)\leq 1$ but this does not allow for any broadening of the solid peaks.

A more general starting point is to take Eq. (20) and allow the "order parameters" ρ_G to vary with z (Ref. 19),

$$\rho(\mathbf{r})=\rho_l+(\rho_s-\rho_l)f_0(z)+\sum_G \rho_G f_G(z)e^{i\mathbf{G}\cdot\mathbf{r}}\,, \qquad (27)$$

where we have introduced an additional variation $f_0(z)$ for the average density change. The interface is now characterized by the manner in which the $f_G(z)$ functions vary from unity deep in the crystal phase to zero in the liquid phase. Quite generally, the $f_G(z)$ of the larger $\mathbf{G}$'s (more rapidly varying Fourier components) must decay to zero over a shorter distance than the $f_G(z)$ associated with smaller $\mathbf{G}$'s since the crystal density is expected to broaden out in the interface. To maintain a positive density is also likely to require that the large G f_G "end" their decay closer to the crystal than those of the smaller G. These features are incorporated by the following scaling form for the "decay length" Δz_G of the order parameter $f_G(z)$:

$$\Delta z_G=|z_G-z_0|=(G_1/G)^{\nu}\Delta z,\quad 0\leq\nu\leq 1,\quad G\geq G_1\,, \qquad (28)$$

where G_1 is the magnitude of the smallest nonzero r.l.v., the parameter Δz is the width of the interface, and the parameter ν controls the rate of broadening of the solid density peaks. We then also take $\Delta z_0=\Delta z$. The order parameters all begin their decay at the same point z_0, although this is another potential variational parameter. Finally, we assume a very convenient shape function for the $f_G(z)$,

$$\begin{aligned} f_G(z)&=1,\quad |z|<z_0 \\ &=\frac{1}{2}\left[1+\cos\left[\pi\frac{z-z_0}{\Delta z_G}\right]\right],\quad z_0<|z|<z_G \\ &=0,\quad z_G<|z| \end{aligned} \qquad (29)$$

for a two-interface slab geometry with the solid phase in $|z|<z_0$, the liquid phase in $|z|>z_0+\Delta z$, and the interfacial variations completely contained in $z_0<|z|<z_0+\Delta z$. Figure 2 shows schematically the behavior of the $f_G(z)$ functions described by Eqs. (28) and (29).

Some particular features of the above parametrization are notable. First, as evident in Eq. (28), the decay lengths Δz_G are all proportional to the full interface width Δz, which is a key aspect in limiting the number of variational parameters. The algebraic scaling in Eq. (28) is motivated by considering the near-crystal region. If

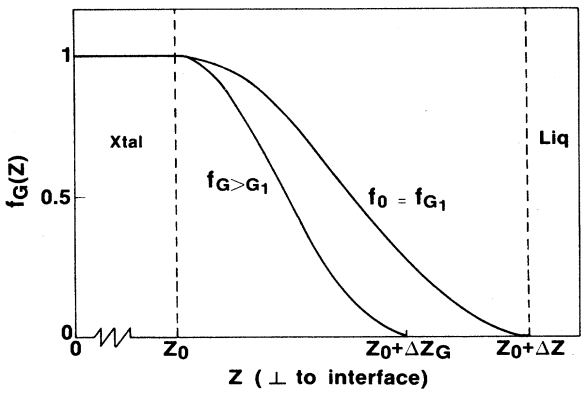

FIG. 2. Schematic of the spatial variations of the $f_G(z)$ order parameters describing the interfacial density profile for an interface of width Δz.

this region were described by simply an $\alpha(z)$ as mentioned earlier, then $\rho_G f_G$ would have behaved as

$$\rho_G f_G(z) \approx \rho_s e^{-G^2/4\alpha(z)} .$$

Equating this $\rho_G f_G(z)$ to an expansion about $z=z_0$ of the $\rho_G f_G(z)$ in Eq. (29), one finds the scaling $\Delta z_G \sim G^{-1}$, i.e., Eq. (28) with $\nu=1$. Algebraic scaling of the Δz_G thus appears appropriate, with a parameter ν monitoring the rate of broadening. Note that $\nu=0$ yields the no-broadening parametrization mentioned earlier. There are several reasons for the choice of the cosine shape functions in Eq. (29). Foremost among them is that these $f_G(z)$ are easily Fourier transformed, which simplifies the subsequent WDA calculations of $\bar{\rho}(\mathbf{r})$ immensely. Also, the interface has a distinct beginning, at $|z_0|$, and end, at $|z_0+\Delta z|$, which simplifies computations and ensures that the two interfaces do not interact even if z_0 is fairly short. In comparison to the usual form of $[1+\tanh\beta(z-z_c)]/2$, the $[1+\sin\beta(z-z_c)]/2$ form [equivalent to Eq. (29) with $z_c=z_0+\Delta z/2$] has exactly the same value and slope at $z=z_c$ and has a 10–90 width only about 20% shorter. So, for the most important region of the interface, the center where the variations are most rapid, Eq. (29) and the "usual" tanh form are *very* similar. Figures 3 and 4 show the planar-averaged interfacial profiles

$$\rho(z)=\frac{1}{A}\int dx\, dy \rho(\mathbf{r})$$

generated by Eqs. (27)–(29) for a variety of $(\Delta z,\nu)$ choices for the fcc (111) interface, with z_0 fixed midway between lattice planes perpendicular to the surface. Values of $\nu \geq 0.8$ show negative densities, and hence $0 \leq \nu \leq 0.75$ is a practical restriction. In general the parametrization spans a range of physically appealing profiles. Aside from changes in lattice plane spacing and a real particle density, the (100) interfaces are very similar (see Fig. 5, for example).

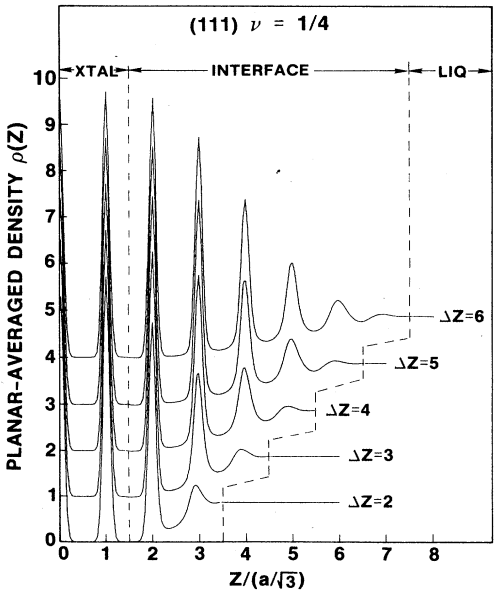

FIG. 3. Planar-averaged interfacial density $\rho(z)$ for the (111) fcc-liquid interface for varying interfacial width Δz at fixed broadening parameter $\nu=0.25$, as generated by the parametrization of Eqs. (27)–(29).

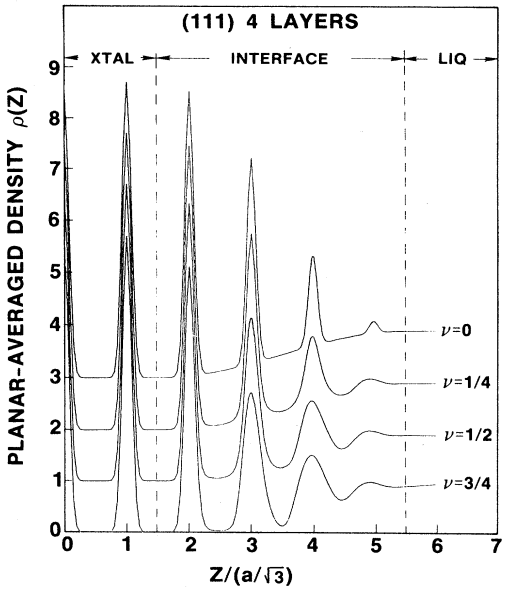

FIG. 4. Planar-averaged interfacial density $\rho(z)$ for the (111) fcc-liquid interface for varying broadening parameter ν at fixed interfacial width Δz=four layers, as generated by the parametrization of Eqs. (27)–(29).

A number of modifications to this parametrization, at the expense of more parameters, are possible. As noted, the quantity z_0 is another parameter and could also be generalized to z_0^G with some scaling form. The variations of $f_0(z)$ and $f_{G1}(z)$ need not be equal since the average density could decay over a width different than Δz. Also, the scaling form of Eq. (28) does not possess anisotropy since r.l.v.'s of the same magnitude decay at the same rate independent of their G_z components. To account for this, Eq. (28) could be generalized to depend on both $\mathbf{G}_\parallel$ and G_z independently. It is important to point out, however, that the lack of anisotropy in the parametrization does not at all preclude anisotropic interfacial properties in a nonlocal density functional theory. Some of the above options may, however, lead to persistent negative density regions and thus be unphysical.

A distinct short-coming of the above parametrization associated with the basic Ansatz of Eq. (27) is that the G vectors are fixed at their bulk crystal values and no spatial fluctuations on other length scales are allowed. This prohibits the inclusion of lattice expansion or contraction into the parametrization. A possible solution to this problem is to allow the lattice parameter a to vary through the interface, although it is not clear how to do this properly. As evident upon careful inspection of some of the profiles in Figs. 3 and 4, the peaks in the densities are slightly shifted toward the *crystal*. This *apparent* con-

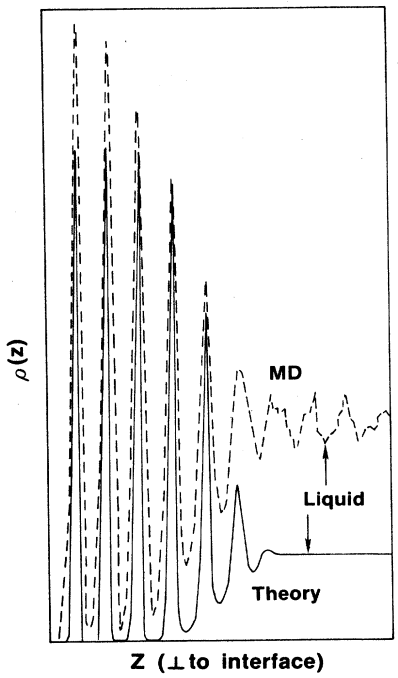

FIG. 5. Equilibrium planar-averaged interfacial density $\rho(z)$ of the (100) fcc-liquid interface. Solid line: present theory for hard spheres, four nonbulk layers. Dashed line: simulation result for soft spheres, six and seven nonbulk layers. The centers of the predicted and simulated profiles have been approximately aligned.

traction, which increases with increasing ν, is basically the consequence of multiplying a symmetric function by an asymmetric one, thereby introducing a slight asymmetry which in this case favors the crystalline side of the broadened peaks. Aside from allowing for an expansion of a, we know of no way to rectify this situation.

B. Hard-sphere interface results

For a chosen crystal face in contact with the coexisting liquid, the interfacial properties are obtained straightforwardly by minimizing Eq. (26), using the WDA for $F_{ex}[\rho]$, with respect to Δz and ν, the two variational parameters describing $\rho(\mathbf{r})$. For the hard-sphere system, we use the Percus-Yevick approximation throughout so that the coexistence conditions are those given in Table II. Some calculational details are provided in the Appendix.

The equilibrium (100) planar-averaged interface is shown in Fig. 5 and has a width of four atomic layers (each layer of width $a/2$), i.e., four layers of neither bulk crystal nor bulk liquid density, with an exponent of $\nu \simeq 0.25$ and a surface free energy of $\gamma = (0.66 \pm 0.02) kT/\sigma^2$. As evident in Fig. 6, which shows $\beta\Delta\Omega/A$ for a variety of $(\Delta z/\nu)$ values, the five-layer interface is only slightly higher in energy and is within the estimated errors of the calculation. Generally, we find the $\nu=0$ (no broadening) density profiles to be significantly higher in free energy than the $\nu=0.25$ profiles, while the broader $\nu=0.5$ profiles are only slightly higher than the $\nu=0.25$ profiles. The variations in $\beta\Delta\Omega/A$ with interface width are similar for the different ν values so that the effects of broadening rate and width are weakly coupled. Since the peaks in the density profile contract slightly with increasing ν, with no contraction at $\nu=0$, the interface seems to prefer some broadening despite the associated expense of the contraction (not seen in simulations). This suggests that if a lattice expansion could be incorporated into the parametrization then equilibrium interfaces with larger ν would be predicted.

The equilibrium (111) planar-averaged interface is also found to consist of four layers (each layer of width $a/\sqrt{3}$) with an exponent of $\nu=0.25$ but a slightly lower surface free energy of $\gamma = (0.63 \pm 0.02) kT/\sigma^2$. The general variations of $\beta\Delta\Omega/A$ with varying Δz and ν are similar to those found for the (100) interface [compare Figs. 6(a) and 6(b)], with the exception that it is the (111) three-layer interface which is very close in energy to the (111) four-layer interface. Layer-by-layer contributions to the surface free energy of the (111) interface are presented in Fig. 7. The largest contributions to γ occur in the middle of the interface where the profile is varying most rapidly as expected. However, the contributions are not symmetric about the center of the interface, the near-crystal region costing more free energy than the near-liquid region. In addition, small but non-negligible contributions to $\beta\Delta\Omega/A$ come from the "bulk" layers adjacent to the interface on each side. These contributions are a consequence of the nonlocal functional, which has a range $\sim\sigma$ that is larger than the interlayer spacings of both the (111) and (100) interfaces.

The interfaces studied here show very little anisotropy

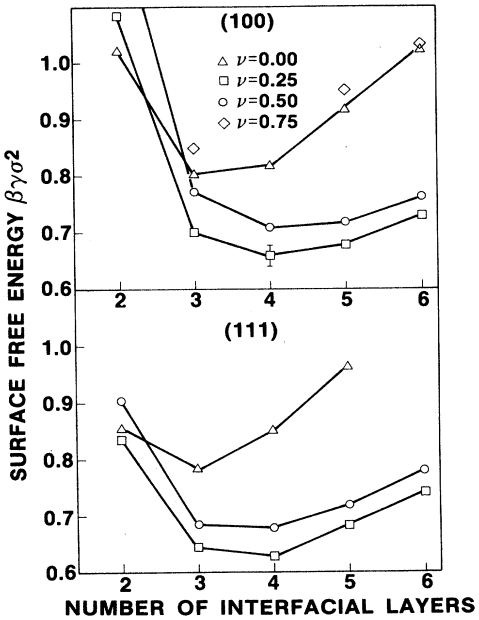

FIG. 6. Surface free energy $\beta\gamma\sigma^2$ vs number of interfacial layers for various values of the broadening parameter ν for the hard-sphere (100) and (111) fcc-liquid interfaces.

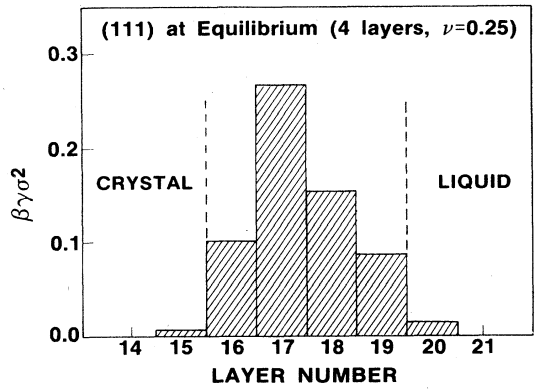

FIG. 7. Layer-by-layer contributions to the surface free energy $\beta\gamma\sigma^2$ of the equilibrium hard-sphere (111) fcc-liquid interface, with the interface located in layers 16–19.

in γ, with $\gamma(111)$ less than $\gamma(100)$ by only about 5%, and some of the difference may reflect uncertainty in the calculated results. In addition, the observed expansion of the (100) planes in the LJ system suggests that if such an expansion could be accomplished here, $\gamma(100)$ would decrease slightly and thereby diminish or even reverse the present trend in anisotropy. Structural differences between the interfaces are also quite small since both have four atomic layers and $\nu \simeq 0.25$. Finally, since both (100) and (111) interfaces are fairly narrow, the full 3D variations in the density are *not* small even in the near-liquid layers. Also, with the scaling of Eq. (28) and $\nu=0.25$, the larger G vectors decay over only about two layers. These observations suggest that the SGA is not applicable and that the use of a nonperturbative, non-SGA functional such as the WDA is necessary to study these interfaces appropriately.

Although simulations on hard-sphere interfaces are not available, we can make some qualitative and quantitative comparisons to the simulations on r^{-12} and LJ potential systems because the steeply repulsive nature of all these potentials is expected to dominate the structures of the crystal, liquid and interface. The r^{-12} interfaces studied by Cape and Woodcock[10] (100) and Tallon[11] (111) and the (100) and (111) LJ interfaces examined by Broughton and Gilmer[9] consist of approximately six or seven atomic layers, with some small density variations apparently extending further into the bulk phases. In direct comparison, our results showing only four layers are thus a bit too narrow. Better agreement with the simulations would likely be found if our shape functions $f_G(z)$ exhibited tails into the "bulk" phases. As noted earlier, the cosine and hyperbolic tangent shape functions are identical near the middle of the interface and only differ significantly near the ends of the interface, where the cosine form terminates abruptly. Since the contributions to γ from the ends of the interface are rather small (see Fig. 7), we expect that profiles with longer tails, but with the same rate of change through the center of the interface, would yield broader width estimates and rather similar values of γ to the results obtained here. For reference, the number of "nonbulk" (densities differing by more than 2% from either bulk phase) layers expected for a tanh-like profile is two more than for the cosine profile for these widths; hence, using the more gradual profile form we might expect "widths" of six layers. In any case, the four-layer width obtained here is still in reasonable agreement. By approximately aligning the centers of the (100) interface profile calculated here with that of the r^{-12} (100) simulations[10] (see Fig. 5), it appears that the basic structural details of the interfaces are quite similar. In particular, our assumption that $f_0(z)=f_{G1}(z)$ appears to be reasonable.

A quantitative comparison of the r^{-12} simulation results with our calculational results is also warranted because of the close similarity of soft and hard spheres. The soft spheres show $\Delta s=1.0$, $L=0.14$, and a comparatively small energy of fusion, indicating again that entropy and short-range repulsion dominate the freezing of this system. To compare our value of γ to the surface stress of the r^{-12} system (which, however, is not identical to γ since the crystal can sustain finite shear stresses) of $(0.46\pm0.1)(kT/\varepsilon)^{1/6}kt/\sigma^2$,[10] we assume that the thermodynamics of a hs sphere system of effective diameter $d/\sigma=(\varepsilon/kT)^{1/n}(1+B/n)$ ($B=0.5772$) can approximate that of the $\varepsilon(r/\sigma)^{-n}$ potential system.[43] Scaling our hs results, we then find $\gamma=0.60(kT/\varepsilon)^{1/6}(kT/\sigma^2)$ in fair agreement with the simulation result. In addition, the ratio of $\beta\gamma\sigma^2$ to Δs, an empirical invariant for a wide range of materials,[3] is found to be 0.46 for the soft spheres and 0.45 for the hard spheres.

C. Lennard-Jones interface results

In this brief section, we extend our simple calculation of Lennard-Jones bulk-phase coexistence to the the interface. Our main goal is to assess the importance of the additional attractive interactions on the interfacial free energy and to compare our results to the simulation values of Broughton and Gilmer.[9] We have already seen in Sec. III B that the structural dependence of the crystal internal energy is not crucial to obtaining reasonable phase boundaries. Since the average density change at the transition is fairly small and is expected to occur over several atomic layers, we modify the attractive contribution to F_{ex}, the third term in Eq. (24), to essentially a local density form. Defining the attractive contribution to the free energy per unit volume as

$$\frac{F_{att}(\rho)}{V}=\tfrac{1}{2}\rho^2\int d\mathbf{r}\,\phi(\mathbf{r})g_{hs}(r;\rho,d)\ , \tag{30}$$

we take the approximate free energy to be

$$F[\rho]=F_{id}[\rho]+F_{ex}^{hs}[\rho]+\frac{1}{L_z}\int_{L_z}dz\,F_{att}(\rho(z)) \tag{31}$$

where $\rho(z)=\rho_l+(\rho_s-\rho_l)f_0(z)$. An alternative and nearly equivalent approximation is that of the SGA applied to $F_{att}(\rho)$, which is expected to be acceptable since the $f_0(z)$ order parameter is fairly slowly varying. The local form in Eq. (31) leads to a preference for narrower interfaces than predicted by $F_{hs}[\rho]$ alone, but narrower interfaces only result if the attractive terms are large enough to counteract the hs contributions to γ. Note also that hav-

ing suppressed any structural dependence to F_{att}, this contribution is isotropic.

We consider $kT/\varepsilon=0.666$ ($d/\sigma=1$) which is close to the triple point conditions found by Broughton and Gilmer ($kT/\varepsilon=0.617$). The bulk-phase coexistence conditions at this point are given in Table III. The attractive contribution to Eq. (26), γ_{att}, is easily calculated from the last term in (31) and the surface free energy is $\gamma_{LJ}=\gamma_{hs}+\gamma_{att}$. From our previous hard-sphere results, we can estimate the hard-sphere contribution as about $0.42\varepsilon/\sigma^2$. The attractive contribution, on the other hand, is only about $+0.016\varepsilon/\sigma^2$ per layer, and hence is considerably smaller in magnitude. So, while the precise result requires the full minimization of γ_{hs} to be carried out at the appropriate LJ coexistence conditions, we restrict the parameter space to $\nu=0.25$ only, since γ_{att} is small and ν independent. We find the hard-sphere contributions to be $\gamma_{hs}=0.37\varepsilon/\sigma^2$ for the four-layer (111) interface and $\gamma_{hs}=0.38\varepsilon/\sigma^2$ for the three-layer (111) interface. Comparing to the results at hard-sphere-coexistence, γ_{hs} is clearly fairly sensitive to the precise coexistence conditions but the ordering is quite similar. Combining these γ_{hs} results with γ_{att}, which slightly favors the narrower interface, we find the three- and four-layer (111) LJ interfaces to have essentially the same surface free energy of $\gamma_{LJ}(111)=0.43\varepsilon/\sigma^2$. The interfacial structure is narrower than observed in the simulation studies but the surface free energies are quite close: The simulation value[9] is $\gamma_{LJ}(111)=0.35\varepsilon/\sigma^2$ so that, as in the scaled r^{-12} case, our predicted results are only about 25% too large. From the above discussion, $\gamma_{LJ}(100)$ is expected to be very nearly equal to $\gamma_{LJ}(111)$.

D. Additional comments

Our results for both hs and LJ interfaces are generally in agreement with simulation studies, with the γ values found here larger than the simulation values. While part of the deviation inevitably lies in our use of the WDA, improved parametrizations will necessarily lower the calculated γ values, by virtue of the variational nature of the calculation, and bring them closer to the simulation values. It is interesting to compare our γ values to Turnbull's empirical relation between γ and the latent heat ΔH of closed-packed metallic elements,[3]

$$\gamma=0.45\Delta H\rho_s^{2/3} . \tag{32}$$

The hs values of γ obey this quite closely, with $\gamma(111)/\Delta H\rho_s^{2/3}=0.43$ and $\gamma(100)/\Delta H\rho_s^{2/3}=0.45$. For the LJ system at $kT/\varepsilon=0.666$, $\Delta H=0.94\varepsilon$ and $\gamma(111)/\rho_s^{2/3}\Delta H=0.45$. This agreement is primarily a consequence of the domination of the hard-sphere part of the free energy and of the close adherence of our hs results to Eq. (32). The agreement of our results with Eq. (32) is fortuitously good, of course, but still interesting and rather remarkable.

V. DISCUSSION

The interfacial properties calculated within the present framework may be compared to a variety of other DFT calculations of crystal-melt interfaces. The most complete study, aside from the present one, is that of McMullen and Oxtoby (MO) (Ref. 47). MO employed the RY-HO truncated expansion combined with several parametrizations *without* any peak broadening to study the fcc hard-sphere interfaces. While they found narrow, isotropic interfaces of about 3σ in width, their values for γ were rather large, $\gamma\approx 1.66kT/\sigma^2$. MO attributed the large γ values to the large latent heat predicted by the RY-HO functional. However, the equilibrium crystal phase in this theory is also much more highly localized ($\alpha\sigma^2=373$ vs $\alpha\sigma^2\approx 90$ in simulations), which may be deleterious to γ. Surprisingly, when MO considered a parametrization that did allow for peak broadening through the interface they found γ values *twice again as large.* This behavior is radically different from that found here, when some broadening ($\nu>0$) does lower γ, and over a wide range of ν the variations in γ are not large compared to the equilibrium value (see Fig. 6). It would be of considerable interest to employ the present parametrization in an RY-HO functional, which would allow for a better assessment of the importance of the functional (although this is still convoluted with the possibly important differences in bulk-phase coexistence predicted by the two functionals). Finally, McMullen and Oxtoby compared their full functional results to those obtained with the additional SGA and found the SGA to be unsatisfactory in detail but acceptable for obtaining approximate results.

Moore and Raveche used a functional similar to the RY-HO functional and a no-broadening parametrization with the SGA to study the fcc LJ interfaces.[48] Their theory was not used to calculate the bulk-phase coexistence, instead they used simulation values as imput to their calculation so that the theory is not entirely self-consistent. Moore and Raveche predicted very broad interfaces of 15 layers with a factor of 3 anisotropy in γ, in clear contrast to simulation results. They did, however, use their formal theory to analyze the planer "capillary-wave" correlations in the interface and found a close analogy to the case of the liquid-vapor interface correlations.

Shih *et al.* started from a Landau-like expansion of $F[\rho]$ to fourth order in ρ_G (Ref. 49). Limiting **G** to the $\{110\}$ set for a bcc lattice (and a few related **G**'s), they used (i) the experimentally obtained density change and heat of fusion to set the expansion parameters, and (ii) a square-gradient approximation for the interface, and predicted a reasonable γ for Na. They also found only small anisotropy and narrow interfaces. Despite its simplicity and very approximate representation of the crystal density, the use of experimental input appears to make this approach useful for easy estimates of γ for a wide variety of systems. In addition, Shih *et al.* were able to derive a relation between γ and ΔH analogous to Turnbull's relation (although for bcc materials) from their theory.

A completely different liquid-based approach to the freezing and crystal-melt interface has been presented by Klupsch.[50] Here, a Percus-Yevick closure equation is used in combination with the general Ornstein-Zernike equation to obtain the pair and direct correlation functions of an *inhomogeneous* liquid. Applying the theory to

the Lennard-Jones system, with an additional hard-core perturbation theory and a "strong localization" condition, reasonable coexistence densities are obtained slightly above the triple point ($kT/\varepsilon=0.752$) but with very strong localization (large α). For the interfacial region, a no-broadening parametrization is used and an interfacial width of about 3.5σ and surface energy of $0.968\varepsilon/\sigma^2$ are obtained, the latter being somewhat *higher* than the simulation values at *lower* temperatures. While this approach is novel and appears useful, the strong localization condition required to solve the coupled integral equations essentially cuts off the tails of the Gaussian densities so that the particles on different lattice sites do not interact with the hard cores of their neighboring particles. Freezing is thus apparently controlled by the ideal gas free energy and the internal energy contributions (similar to the contributions in the Debye theory), and the structure of the crystal-melt interface is controlled mainly by the attractive part of the potential, in contrast to our results. Finally, with the apparent absence of any appreciable excess entropy due to the strong localization condition, hard spheres might not freeze using this approach.

The limitations of all of the density functional theories discussed above, including mainly the truncated functional expansion and very limited density parametrizations, are overcome by the approach taken in the present work. The equilibrium bulk-phase coexistence and crystal $\rho_s(\mathbf{r})$ are in good agreement with simulation, an SGA is unnecessary, and the density parametrization allows for peak broadening in a controlled manner. Our generally good agreement with simulation data indicates that some, if not all, of these aspects are important in studying crystal-melt interfaces. The parametrization presented here does have its limitations as noted earlier but nonetheless it provides a foundation for even more sophisticated representations of the interfacial profile. The WDA also has limitations; it is primarily useful as an excess entropy functional, which is why hard-sphere perturbation theory was utilized to study the LJ potential. This poses some problem in extending the WDA theory to simple metal interfaces. Namely, in metallic systems the effective pair potential is density dependent, because of the density-dependent electron screening of the ion cores, and since there is an average density change through the crystal-liquid interface there is a corresponding potential variation and an effective hard-sphere diameter variation. Fortunately, the electronic contributions to the free energy cause the density change to be much smaller than in the LJ and hs liquids, and hence a density-independent diameter may not be a poor approximation, but this has yet to be tested. The problem of density-dependent potentials actually also exists in application of the usual RY-HO functional but is implicit, and thus hidden, in the theory: The liquid $c^{(2)}$ corresponding to the liquid-density potential $\phi(\rho_l)$ is assumed an adequate approximation to the crystal with its *different* potential $\phi(\rho_s)$. This issue has not been addressed even though many of the applications of the RY-HO theory are ostensibly to metallic systems.[19]

The DFT of the crystal-liquid interface is intrinsically a theory for the *equilibrium* interface. As such, it is difficult to see precisely how it might be utilized for investigating growth, i.e., nonequilibrium, phenomena aside from providing the necessary equilibrium-state information such as ΔH and γ required in existing growth theories. One possible avenue is to use the DFT to estimate the free energy barriers between equilibrium states by assuming that the free energy functional evaluated at a density configuration away from the minimum may be interpreted as the free energy of that configuration. For the crystal-melt interface, equivalent equilibrium states are related via a translation of the interface by an integral number of lattice planes perpendicular to the interface. This corresponds to a translation of z_0 in our parametrization, and the surface free energy shows both the minima associated with equilibrium states and maxima somewhere between these states. The difference between maximum and minimum values is taken to represent the free energy barrier $\Delta\gamma$. In Cahn's model of crystal growth from the melt, $\Delta\gamma$ determines a critical undercooling ΔT^* below which ($\Delta T<\Delta T^*$) the crystal grows in an activated over-the-barrier manner and above which ($\Delta T^*<\Delta T$) the crystal growth proceeds continuously.[51] This behavior is similar to that of a charge density wave exhibiting a washboard potential and in the presence of an electric field: a critical field exists above which the CDW slides without activation. We have estimated $\Delta\gamma$ for the hard-sphere (111) interface by considering z_0 as a continuous parameter and have examined two values of z_0, at the midpoint between lattice planes and at the lattice planes themselves. We find the midpoint z_0 to be the minimum and obtain a value of $\Delta\gamma/\gamma\simeq 0.007$. If this value is used to estimate the critical undercooling, we find $\Delta T^*\approx(0.003)T_M$. Such a small critical undercooling (it is probably even smaller, given the accuracy of our calculations) is consistent with the generally observed continuous growth of simple metals and, in Jackson's language, low-α materials in general. An alternative to the above simple translation of the interface during growth is an "inch-worm" motion. In this case, the four-layer interface first extends to five layers by adding an extra layer in the liquid side or contracts to three layers by subtracting the first noncrystalline layer. Subsequently the interface contracts or extends, respectively, to reestablish a four-layer interface translated one layer into the liquid. $\Delta\gamma/\gamma$ can then be obtained directly from Fig. 4 and we find $\Delta\gamma/\gamma\approx 0.01-0.02$, which is larger than found above and suggests that uniform translational motion is preferred. While the critical undercooling ΔT^* predicted is fairly small, as expected, one must remember that the entire procedure is predicated on the assumption that the density functionals have a physical interpretation away from equilibrium. We also neglect other kinetic aspects of the growth process which have recently been seen in simulation studies. Specifically, the (100) LJ interface has been found to grow without activation, as suggested by the above discussion, but growth of the (111) LJ interface is apparently activated and a concerted motion of many atoms is required to advance this interface.[6] It is unlikely that any DFT will be capable of predicting such subtle phenomena.

Surface melting, on the other hand, is an equilibrium

phenomenon which could be analyzed by the general method discussed in this paper. Low index crystal planes at the crystal-liquid interfaces of Pb have been observed to melt below the bulk melting point T_M, with the thickness of the liquid layer diverging as T_M is approached[52] and similar behavior for Aluminum has recently been observed in a simulation study.[53] For "liquidlike" layers only a few atomic diameters in width, the proximity of the crystal-liquid and liquid-vapor interfaces must affect the thermodynamics of the system. With a suitable density parametrization, and perhaps hard-sphere perturbation theory, the WDA is capable of analyzing these inhomogeneous systems in a straightforward manner. The simple parametrization given here with $\nu=0.0$ and Δz the only parameter (taking on continuous values $\Delta z \geq 0$) should be a useful starting point for estimating the temperature at which the surface first melts. The structure at temperatures approaching T_M is less abrupt and so easier to describe. We thus expect that the initiation and propagation of surface melting is approachable, albeit still within mean-field theory, using the WDA.

In summary, the weighted-density functional approximation to the excess Helmholtz free energy of an inhomogenous liquid has been shown to yield good predictions for the structure and surface free energy of simple crystal-melt interfaces. The accuracy of our results is due not only to the accuracy of the WDA in predicting the bulk-phase coexistence but also to the use of a flexible parametrization of the crystal-melt interfacial density profile which includes broadening of the crystal density peaks on entering the interfacial region. Modifications to the parametrization and to the manner in which attractive interparticle interactions are included have been suggested, which should lead to even better results than obtained here. With the successful application of the WDA to both simple[27,28] and binary[54] liquid freezing, crystal elastic constants,[55] wetting and capillary condensation,[30] submonolayer gas condensation on surfaces,[56] and now the crystal-melt interface, the WDA provides the most versatile and accurate description of inhomogeneous liquids at the present time, since no other single functional (e.g., the local-density functional or the RY-HO functional) has shown the capability of dealing with such a broad spectrum of phenomena. Future applications of the WDA to, for instance, nonspherical molecular fluids, surface melting, and grain boundary structures, appear to require only minor generalizations or modifications of the basic theory and flexible parametrizations in the spirit of the parametrization presented here.

ACKNOWLEDGMENTS

The author wishes to thank J. Kerins, L. A. Turkevich, H. Scher, and N. W. Ashcroft for useful discussions during the course of this work.

APPENDIX

In this brief appendix, we discuss the numerical procedures used to evaluate the self-consistent weighted-density $\bar{\rho}(\mathbf{r})$ and, subsequently, the excess Helmholtz free energy. For the interface problem, the broken symmetry relative to the crystalline phase divides each set of reciprocal lattice vectors $\{\mathbf{G}\}$ equivalent by symmetry in the crystal into subsets $\{\mathbf{G}_\parallel, G_z\}$, where $\hat{z}$ is the normal to the plane of the interface (which is not necessarily along a cubic axis of the crystal). Thus, the calculation of $\bar{\rho}$ is more complicated than the simple form of Eq. (21) in the main text. Defining the Fourier transforms of $w(r;\bar{\rho}(\mathbf{r}))$ and $f_G(z)$ by

$$w(k;\bar{\rho}(\mathbf{r}))=\int_{-\infty}^{\infty} d\mathbf{r}\, e^{-i\mathbf{k}\cdot\mathbf{r}} w(r;\bar{\rho}(\mathbf{r})) \tag{A1}$$

and

$$f_G(k)=\int_{-\infty}^{\infty} dz\, e^{-ikz} f_G(z) = \frac{\beta_G^2}{k(\beta_G-k)(\beta_G+k)}[\sin(kz_G)+\sin(kz_0)] , \tag{A2}$$

where $\beta_G=\pi/(z_G-z_0)$, we may express $\bar{\rho}(\mathbf{r})$ as

$$\bar{\rho}(\mathbf{r})=\rho_l+(\rho_s-\rho_l)\frac{1}{2\pi}\int dk_z e^{-ik_z z} w(k_z) f_0(-k_z) + \sum_G \rho_G e^{i\mathbf{G}_\parallel\cdot\mathbf{R}} \frac{1}{2\pi} \times \int dk_z e^{-ik_z z} w((\mathbf{G}_\parallel^2+k_z^2)^{1/2}) f_G(k_z+G_z) , \tag{A3}$$

with $\mathbf{R}$ the component of $\mathbf{r}$ perpendicular to $\hat{z}$. Now for each $(\mathbf{G}_\parallel, G_z)$, there is a vector $(-\mathbf{G}_\parallel, -G_z)$ and since w and f are even functions of wave vector, the last term in (A3) may be rewritten as (changing k_z to simply k)

$$= \sum_{\mathbf{G}_\parallel} \frac{1}{\pi}\int dk\, w((\mathbf{G}_\parallel^2+k^2)^{1/2}) \left[\left[\sum_{\{\mathbf{G}_\parallel\}} \cos(\mathbf{G}_\parallel\cdot\mathbf{R}) \right] \cos(kz) \left[\sum_{G_z} \rho_G (f_G(k+G_z)+f_G(k-G_z)) \right] + \left[\sum_{\{\mathbf{G}_\parallel\}} \sin(\mathbf{G}_\parallel\cdot\mathbf{R}) \right] \sin(kz) \left[\sum_{G_z} \rho_G (f_G(k+G_z)-f_G(k-G_z)) \right] \right] . \tag{A4}$$

Here, the sums over G_z are over all positive G_z which can be associated with a particular magnitude of $\mathbf{G}_\parallel$, the sums over $\{\mathbf{G}_\parallel\}$ are over those vectors equivalent by symmetry and having the same magnitude $\mathbf{G}_\parallel$, and the sum over $\mathbf{G}_\parallel$ is over all magnitudes of $\mathbf{G}_\parallel$. Notice that for a fixed interface profile that the two sums over G_z in (A4) need only be calculated *once* since they are $\mathbf{r}$ independent. Furthermore, only w in (A4) depends on $\bar{\rho}(\mathbf{r})$, although the dependence is not shown explicitly. So, at each point $\mathbf{r}$ the entire term in [ ] is calculated only *once*. Computa-

tions are still lengthy, however, since at each $\mathbf{r}$ point the one-dimensional Fourier transform over k must be performed for each value of $\mathbf{G}_{\|}$, the results summed together, a non-self-consistent value of $\bar{\rho}(\mathbf{r})$ calculated and then the entire procedure iterated to self-consistency. Subsequently, the 3D integral over $\mathbf{r}$ ($\mathbf{r}$ confined to the near-interface region) must be carried out.

To accomplish the above program efficiently, look-up tables are generated for the weight function $w(k;\rho)$ with a k mesh of $0.1/\sigma$ and a ρ mesh of $0.02/\sigma^3$. The integral over k is performed using Simpson's rule with a step size δk, and the z integral through the interface is also performed using Simpson's rule with step size δz. For these fixed mesh sizes, look-up tables of $\cos(kz)$ and $\sin(kz)$ are then calculated. At fixed $\mathbf{R}$, the z integral is evaluated at successive points z, $z+\delta z$ so that the initial estimate of the weighted density at $z+\delta z$, $\bar{\rho}_{\text{init}}(\mathbf{R},z+\delta z)=\bar{\rho}(\mathbf{R},z)$, is close to the correct value. Then, only five iterations are required to obtain sufficient self-consistency of $\bar{\rho}(\mathbf{R},z+\delta z)$. For the (100) interface, we obtained good accuracy for step sizes $\delta k=2\pi/163\sigma$ and $\delta z=a/32$, with a the cubic cell length. For the (111) interface, we found equivalent accuracy could be obtained with $\delta k=6\pi/163\sigma$ and $\delta z=a/20$. In both cases, the subsequent $\mathbf{R}$ integration was performed using a Chebychev polynomial integration routine (kindly provided by C.M.M. Nex of the Cavendish Laboratory, Cambridge University) with up to 32 points for each of the x and y integrations. By symmetry, the $\mathbf{R}$ domains can be reduced to the minimum area regions of ($0<x<a/4$, $y<x$; $a/4<x<a/2$; $y<a/2-x$) for the (100) interface and ($0<x<a/2\sqrt{2}$, $-x/\sqrt{3}<y<x/\sqrt{3}$) for the (111) interface, with the (111) interface axes defined as $\hat{x}=(-1,1,0)/\sqrt{2}$, $\hat{y}=(-1,-1,2)/\sqrt{6}$ and $\hat{z}=(1,1,1)/\sqrt{3}$ relative to the cubic axes.

With this procedure, we calculate free energies for the coexisting crystal phase that agree with our previous results, which use Eq. (21) and different numerical procedures, to within 1 part in 10^4. We thus expect this procedure to be sufficiently accurate through the interface since the density variations become less rapid.

[1]G. Wulff, Z. Kristallophys. **34**, 449 (1901).

[2]W. W. Mullins and R. F. Sekerka, J. Appl. Phys. **34**, 323 (1963); **35**, 344 (1964); J. S. Langer, Rev. Mod. Phys. **52**, 1 (1980).

[3]D. Turnbull, J. Appl. Phys. **21**, 1022 (1950).

[4]K. A. Jackson, *Liquid Metals and Solidification* (ASM, Cleveland, 1958), p. 174.

[5]M. E. Glicksman and C. Vold, Acta Metall. **17**, 1 (1969).

[6]E. Burke, J. Q. Broughton, and G. H. Gilmer, J. Chem. Phys. **89**, 1030 (1988).

[7]E. Ben-Jacob, N. Goldenfeld, J. S. Langer, and G. Schon, Phys. Rev. A **29**, 330 (1984).

[8]L. F. Rull and S. Toxvaerd, J. Chem. Phys. **78**, 3273 (1983).

[9]J. Q. Broughton and G. H. Gilmer, J. Chem. Phys. **84**, 5759 (1986); **84**, 5749 (1986).

[10]J. N. Cape and L. Woodcock, J. Chem. Phys. **73**, 2420 (1980).

[11]J. Tallon, Phys. Rev. Lett. **57**, 1328 (1986).

[12]D. P. Woodruff, *The Solid-Liquid Interface* (Cambridge University Press, London, 1973).

[13]R. H. Ewing, J. Cryst. Growth **11**, 221 (1974).

[14]D. Kuhlmann-Wisdorf, Phys. Rev. **140**, A1599 (1965); R. M. J. Cotterill, E. J. Jensen, and W. D. Kristensen, Phys. Lett. **44A**, 127 (1973).

[15]W. Sutherland, Philos. Mag. Ser. 5 **32**, 31 (1891); **32**, 215 (1891); **32**, 524 (1891); F. A. Lindemann, Phys. Z. **11**, 609 (1910).

[16]P. Platzmann and H. Fukuyama, Phys. Rev. B **10**, 3150 (1974).

[17]D. Stroud and N. W. Ashcroft, Phys. Rev. B **5**, 371 (1972); Equation (23) is missing a factor of 4 in front of the $I(\Theta_D/T)$ term.

[18]T. V. Ramakrishnan and M. Youssouff, Phys. Rev. B **19**, 2775 (1979).

[19]A. D. J. Haymet and D. W. Oxtoby, J. Chem. Phys. **74**, 2559 (1981); **76**, 6262 (1982).

[20]N. D. Mermin, Phys. Rev. **137**, A1441 (1965).

[21]B. B. Laird, J. D. McCoy, and A. D. J. Haymet, J. Chem. Phys. **87**, 5449 (1987); C. Marshall, B. B. Laird, and A. D. J. Haymet, Chem. Phys. Lett. **122**, 320 (1985).

[22]Y. Singh, J. P. Stoessel, and P. G. Wolynes, Phys. Rev. Lett. **54**, 1059 (1985).

[23]S. Sachdev and D. Nelson, Phys. Rev. B **32**, 1480 (1985).

[24]M. Jaric and U. Mohanty, Phys. Rev. Lett. **58**, 230 (1987); G. L. Jones, Mol. Phys. **61**, 455 (1987).

[25]T. V. Ramakrishnan, Phys. Rev. B **37**, 1936 (1988).

[26]W. A. Curtin, J. Chem. Phys. **88**, 7050 (1988).

[27]W. A. Curtin and N. W. Ashcroft, Phys. Rev. A **32**, 2909 (1985).

[28]W. A. Curtin and N. W. Ashcroft, Phys. Rev. Lett. **56**, 2775 (1986).

[29]M. Baus and J. L. Colot, Mol. Phys. **55**, 653 (1985).

[30]P. Tarazona, Mol. Phys. **52**, 81 (1984); Phys. Rev. A **31**, 2672 (1985); P. Tarazona, U. M. B. Marconi, and R. Evans, Mol. Phys. **60**, 573 (1987); P. C. Ball and R. Evans, *ibid.* **63**, 159 (1988).

[31]W. A. Curtin, Phys. Rev. Lett. **59**, 1228 (1987).

[32]R. Evans, Adv. Phys. **28**, 143 (1979).

[33]W. A. Curtin and N. W. Ashcroft, Phys. Rev. Lett. **59**, 2385 (1987).

[34]J. L. Barrat, J. P. Hansen, and G. Pastore, Phys. Rev. Lett. **58**, 2075 (1987).

[35]A. D. J. Haymet, J. Chem. Phys. **78**, 4641 (1983).

[36]See the first reference in Ref. 21.

[37]E. Thiele, J. Chem. Phys. **39**, 474 (1963); M. Wertheim, Phys. Rev. Lett. **19**, 321 (1963).

[38]R. S. Jones and N. W. Ashcroft, J. Chem. Phys. **80**, 3328 (1984).

[39]K. Runge (unpublished).

[40]S. M. Foiles and N. W. Ashcroft, J. Chem. Phys. **75**, 3594 (1981).

[41]N. W. Ashcroft and D. C. Langreth, Phys. Rev. **159**, 500 (1967).

[42]J. P. Hansen and L. Verlet, Phys. Rev. **184**, 151 (1969).

[43]J. P. Hansen and I. R. MacDonald, *Theory of Simple Liquids* (Academic, New York, 1976).

[44]P. F. Choquard, *The Anharmonic Crystal* (Benjamin, New York, 1967).

[45]This comparison was first made by W. A. Curtin, Ph.D. thesis, Cornell University, 1986.
[46]C. Ebner, W. F. Saam, and D. Stroud, Phys. Rev. A **14**, 2264 (1976); also see Ref. 32.
[47]W. E. McMullen and D. W. Oxtoby, J. Chem. Phys. **88**, 1967 (1988).
[48]S. M. Moore and H. J. Raveche, J. Chem. Phys. **85**, 6039 (1986).
[49]W. H. Shih, Z. Q. Wang, X. C. Xeng, and D. Stroud (unpublished).
[50]T. Klupsch, Ann. Phys. (Leipzig) **7**, 179 (1982); Phys. Status Solidi B **109**, 535 (1982).
[51]J. W. Cahn, Acta Metall. **8**, 554 (1960).
[52]J. W. M. Frenken and J. F. van der Veen, Phys. Rev. Lett. **54**, 134 (1985).
[53]P. Stoltze, J. K. Norskov, and U. Landman, Phys. Rev. Lett. **61**, 440 (1988).
[54]A. R. Denton and N. W. Ashcroft (unpublished).
[55]E. Velasco and P. Tarazona, Phys. Rev. A **36**, 979 (1987).
[56]L. Mederos, P. Tarazona, and G. Navascues, Phys. Rev. B **35**, 3376 (1987); **35**, 3384 (1987).